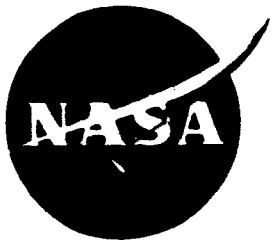

# ATMOSPHERIC TRANSITION CURVES

# FOR

# GEOMAGNETICALLY-SENSITIVE COSMIC RAYS

By

**Robert C. Good, Jr.**



prepared for

**NATIONAL AERONAUTICS AND SPACE ADMINISTRATION**

Contract NAS 1-5254



SPACE SCIENCES LABORATORY

GENERAL ELECTRIC

MISSILE AND SPACE DIVISION

# ATMOSPHERIC TRANSITION CURVES

# FOR

# GEOMAGNETICALLY-SENSITIVE COSMIC RAYS

FINAL REPORT - MARCH, 1966

BY

ROBERT C. GOOD, JR.
GENERAL ELECTRIC SPACE SCIENCES LABORATORY
VALLEY FORGE SPACE TECHNOLOGY CENTER
P. O. BOX 8555 - PHILADELPHIA 1, PENNSYLVANIA

FOR

CONTRACT NO. NAS 1-5254
NATIONAL AERONAUTICS AND SPACE ADMINISTRATION
LANGLEY RESEARCH CENTER
LANGLEY STATION
HAMPTON, VIRGINIA

## ABSTRACT



An attempt is made to reduce some existing observational data on the nuclear cascade in the atmosphere to a form suitable for comparison with nuclear cascade calculations. This data reduction consists in removing from the observational data the contribution of primaries whose energies are too high to permit the cascades they indicate to be calculated with confidence. The procedure is similar to, though simpler than, that used in deriving specific yield functions for use in cosmic ray physics. The results are presented in a family of curves. There is an indication that the number of neutrons at any given depth in the atmosphere is not a sensitive function of the incident rigidity between $\approx 10$ and $\approx 15$ GV. Prescriptions for comparing calculations with these or similar curves are given. Appendix B contains some illustrative curves for incident $\alpha$ particles.

TABLE OF CONTENTS

LIST OF ILLUSTRATIONS

# I. INTRODUCTION

In recent years, much effort has been devoted to the study of the passage of high energy protons in dense matter (nuclear cascade). Such investigations are fundamental to the physics of shielding and dosimetry of solar and non-solar cosmic rays (Ref. 1) and of particles from high energy accelerators (Ref. 2).

On the theoretical side, a number of calculations of the development of the nuclear cascade in thick absorbers have been undertaken by various authors (e.g., Ref. 2, 3, 4). These calculations (hereafter called "cascade calculations") start from available empirical or semi-empirical data on the interactions between individual nucleons and pions. The cascade calculations then go through the knock-on and evaporation stages of each nucleon-nucleus and pion-nucleus interaction in the absorber and follow each secondary produced in these reactions until it interacts, decays, escapes from the absorber, or is captured. The results of these elaborate computations, often employing the Monte-Carlo technique, can then be compared with the corresponding measurements on the nuclear cascade.

On the experimental side, several measurements have been conducted in recent years by various groups at high energy accelerators (e.g., Ref. 5, 6). Usually, a beam of high energy protons is allowed to strike a thick absorber. Detectors of various kinds are used to measure the particles found at various positions inside the absorber. The incident particles (primaries) on the absorber are almost always monoenergetic. Comparison between the experimental results and the calculational results mentioned above has proved satisfactory in some cases and not in others (Ref. 2, 3, 4, 7).

Despite these recent experimental investigations at high energy accelerators, there is a lack of experimental data with which cascade calculations can be meaningfully compared. A question naturally arises: is the vast store of existing empirical data on cosmic-ray-induced nuclear cascades in the atmosphere amenable to comparison with nuclear cascade calculations? One of the difficulties here is that the measured atmospheric nuclear cascades are initiated, not by monoenergetic primary cosmic rays, but by primary cosmic rays having a spectrum of energies, ranging from about 0.5 GeV upwards. Unfortunately, knowledge of nuclear interactions at tens of GeV is so incomplete that, one is able to calculate only in a very speculative fashion the nuclear cascades initiated

by particles above, say, 10 GeV. Thus, comparison with cascade calculations will be fruitful if one can elimin ate from the measured data on atmospheric cascades those cascades initiated by the higher energy primaries. This elimination of atmospheric cascades due to higher energy primaries can indeed be carried out in an approximate manner by using the Earth's field as a magnetic spectrometer. This is entirely similar to the method used by cosmic ray physicists to obtain the "specific yield functions" for cosmic rays in the atmosphere (Ref. 8, 9, 10). Details of the method will be discussed in Section II. To be sure, the primary energy spectrum being a steep inverse power law, the number of primaries above the highest geomagnetic cutoff ($\sim$ 15 GV) is relatively small. However, the expected but unknown increase in the intensity of the nuclear cascade with incident energy probably so reduces this advantage that the effect in the atmosphere of those primaries just above the highest geomagnetic cutoff is not negligible.

The aim of the present report is to try to reduce, in the manner just mentioned, some existing atmospheric data to a form suitable for comparison with cascade calculations that can be realistically undertaken in the near future. It is not our aim here to derive specific yield functions of the kind useful in drawing conclusions about the rigidity dependence of the time-variations of primaries from observations deep in the atmosphere. The latter endeavor would require more elaborate procedures than employed here. The results obtained in the present work contain uncertainties which are believed to be not greater than the uncertainities likely to be encountered in cascade calculations in the near future. The procedure illustrated is applicable not only to the data treated, but also to future measurements of the nuclear cascade in the atmosphere.

Certain analytical steps usual in the derivation of specific yield functions (Ref. 8, 9, 10) for cosmic-ray use are omitted. The reason for these simplifications is that the cascade calculations can more readily and more accurately take into account the geometrical and kinematical complexities than can be done here. For example, in the present report, the Gross transformation (Ref. 9) is not applied to the atmospheric data, the versatile cascade calculations making the transformation unnecessary. Also, no assumption is made here concerning the nature of nuclear cascades induced by primary nuclei heavier than the proton. Such an assumption, if still needed later, can be made when the cascade calculations are performed. These simplifications are discussed in Section IV.

## II. FORMALISM

In general, cosmic-ray measurements made in the atmosphere give the magnitude $I(x, R)$ of the detected quantity as a function of the atmospheric depth $x$ and of the cutoff rigidity $R$ (corresponding to geomagnetic latitude $\lambda$). The measured quantity may be the flux of 1 to 5 MeV neutrons, or the absorbed dose rate in tissue, or beryllium-7 production rate in air, or some other entity. It is assumed that the cutoff rigidity is unique for a given geomagnetic latitude. For convenience, the vertical cutoff rigidity may be taken as this unique cutoff rigidity.

It is customary to plot $I(x, R)$ as a function of $x$ for various $R$; the resulting curves are usually called the transition curves. Alternatively, one may plot $I(x, R)$ as a function of $R$, using $x$ as the parameter; the resulting curves are the latitude curves.

$I(x, R)$ represents the combined effect at depth $x$ of primary cosmic rays of all rigidities above $R$. Hence, we can write

$$\frac{dI(x,R)}{dR} = S(x,R) \quad \frac{dJ(R)}{dR} \tag{1}$$

where $\frac{dJ(R)}{dR}$ is the differential rigidity spectrum of the primaries, $J(R)$ being the integral spectrum. $S(x, R)$ is called the "specific yield function" for the detected quantity in question (e. g. 1 to 5 MeV neutrons). $S(x, R)$ is a quantity properly belonging to nuclear physics, in the sense that it is independent of the intensity and spectral shape of the primaries. We seek $S(x, R)$ or some quantity akin to it for comparison with cascade calculations.

It is customary to graph $S(x, R)$ as a function of $R$, using $x$ as a parameter. Alternatively, one may graph $S(x, R)$ as a function of $x$, using $R$ as a parameter.

Actually, the situation is more complicated, since primary cosmic rays contain nuclei of various mass numbers and atomic numbers. Ignoring the isotopic composition and retaining only the elemental composition, we can rewrite Equation (1) as follows:

$$\frac{dI(x,R)}{dR} = S_Z(x,R)\ \frac{dJ_Z(R)}{dR} \qquad (2)$$

where the subscripts Z refer to primaries of atomic number Z. Unfortunately, $S_Z(x,R)$ cannot be determined from Equation (2).

We will describe two methods for obtaining some information about $S_Z(x,R)$. Method 1 is the one we will adopt in this report as the more convenient for the purpose of securing data for comparison with cascade calculations. Method 2, which we will not use, is more appropriate for deriving specific yield functions for use in studying the rigidity dependence of primary cosmic rays. (See Appendix B).

Method 1: We define an "average specific yield function per cosmic-ray nucleon" $\overline{S}_n(x,R)$:

$$\overline{S}_n(x,R) = \frac{dI(x,R)}{dR} \Big/ \frac{dJ_n(R)}{dR} \qquad (3)$$

where

$$J_n(R) = \sum_Z A_Z J_Z(R) \qquad (3.1)$$

is the primary integral rigidity spectrum weighted by the mass number $A_Z$ of the various charge components. Let us define $N_Z(R)$ as the fractional nucleon abundance of component Z at rigidity R. That is,

$$N_Z = \frac{A_Z\ \frac{dJ_Z(R)}{dR}}{\frac{dJ(R)}{dR}} \qquad (4)$$

The relationship between $\overline{S}_n$ and $S_Z$ is therefore:

$$\overline{S_n}(x,R) = \sum_z S_z(x,R)\, N_z(R)/A_z \qquad (5)$$

It should be noted that $\overline{S_n}$ is averaged over the various charge components of the primaries for any given rigidity. In particular, $\overline{S_n}$ is not the same as $S_{z=1}$.

Method 2: Assume that the nuclear cascade induced by a primary nucleus of mass number A is equivalent to the superposition of A nuclear cascades induced by A single free nucleons each having the same velocity as the individual nucleons in the primary nucleus. Since the mass-to-charge ratio (A/Z) of all nuclei heavier than hydrogen is roughly equal to 2, the above assumption may be written as:

$$S_Z(x,R) = A_z S_1(x, \tfrac{1}{2} R), \text{ for all } Z \geq 2 \qquad (6)$$

where $S_1$ is the abbreviation for $S_{z=1}$. In the above, it is also implicitly assumed that deuterons and tritons are to be counted as protons and $He^3$ is to be counted as $He^4$. Then,

$$\frac{dI}{dR} = S_1(x,R)\,\frac{dJ_1(R)}{dR} + S_1(x,\tfrac{1}{2}R) \sum_{Z \geq 2} A_Z \frac{dJ_z(R)}{dR} \qquad (7)$$

Knowing $J_1(R)$, $J_2(R)$, etc., and I(R,x), one can find $S_1(x,R)$ from Equation (7) using the method of successive approximations exemplified in Ref. 10. $S_Z$ for $Z \geq 2$ can then be found using Equation (6).

As already stated, Method 1 will be used in the main text of this report. Method 2 will be used in Appendix B to obtain some illustrated data on $S_z(x,R)$ for Z = 1 and Z = 2.

Strictly speaking, in order to eliminate the contribution of higher energy primaries, it is only necessary to seek $\frac{dI}{dR}$. It is not necessary to normalize by dividing by $\frac{dJ(R)}{dR}$.

as in Equation (3). We will nevertheless seek $\overline{S_n}$ instead of just $\frac{dI}{dR}$.

Our adoption of Method 1 does not mean that we have altogether avoided making the assumption made in Method 2, riz., that a nucleus of mass number A is equivalent to A free nucleons as far as cascade production is concerned. We have simply postponed making this assumption or some other assumption concerning the interaction of heavy cosmic rays with the atmosphere until the time when cascade calculations are to be made. Present knowledge on high-energy nucleus-nucleus interactions is so fragmentary that the simple but probably unrealistic assumption in Method 2 is often made for lack of a better one. In fact, the assumption of Method 2 amounts to saying that a cosmic-ray nucleus of mass number A invariably breaks up into A free nucleons in a distance negligible compared with the characteristic length of the initial region of the typical atmospheric transition curve. It is hoped that more realistic ways of handling the nuclear cascade induced by heavy nuclei (esp. $\alpha$ particles) can be brought to bear by the time the cascade calculations are performed.

## III. PROCEDURES AND RESULTS

From empirical data, we obtain $I(x, \lambda)$ and $J_n(\lambda)$ for the same epoch in the solar cycle. Using Equation (3), we then obtain $S_n(x, \lambda)$. Instead of cutoff rigidity R, we will use the geomagnetic latitude $\lambda$, assuming a unique R exists for a given $\lambda$ (see Section IV for a discussion).

For solar-minimum $J_n(\lambda)$, we use the relative latitude curve of primary protons measured in a satellite in 1961 by Albert et. al. (Ref. 11). This latitude curve has been adjusted to the solar minimum of 1954 by Lingenfelter (Ref. 12) using the 11-year time-variation data of Neher and Anderson (Ref. 13) and of Lockwood (Ref. 14). Finally, this primary latitude curve was appropriately normalized to the cosmic-ray measurements of Explorer 7 (Ref. 15) and Mariner B (Ref. 16).

$I(x, \lambda)$, for the production rate of neutrons, is taken from the semi-empirical data of Lingenfelter (Ref. 12) at solar minimum. These data are based on the measurements of Soberman (Ref. 17), Rose et. al. (Ref. 18), Simpson and Fagot (Ref. 19), Simpson (Ref. 20), Meyer and Simpson (Ref. 21), and on the star production data of Lord (Ref. 22). The left ordinate of Figure 1 gives the resulting $S_n(x, \lambda)$ for neutron production in air plotted here as a function of atmospheric depth x, using the geomagnetic latitude $\lambda$ as parameter. Figure 2 is a replot of the data in Figure 1 as a function of $\lambda$, using x as parameter.

$I(x, \lambda)$, for the production of stars of one or more prongs is taken from the data in Shen (Ref. 23) for Solar Minimum. These data are based on Lingenfelter (Ref. 12) and Lal et. al (Ref. 24), and normalized to the absolute star rate measured in cloud chambers at mountain altitudes. (See References 23a and 23b.) The right ordinates of Figures 1 and 2 give the resulting $S_n$ for star production in air.

$I(x, \lambda)$, for the RBE dose rate due to neutrons, is taken from the data given by Shen (Ref. 23) for solar minimum. These data were in turn based on the semi-empirical data of Lingenfelter (Ref. 21), Lal et. al. (Ref. 24), Haymes et. al. (Ref. 25), and on the dose calculations of Patterson et. al. (Ref. 26). Figure 3 gives the resulting $S_n(x, \lambda)$ for neutron RBE dose as a function of atmospheric depth x, using geomagnetic latitude $\lambda$ as parameter. Figure 4 is a replot of the data in Figure 3 as a function of $\lambda$ with x as the parameter.

$I(x, \lambda)$, for the production rate of carbon-14 in the atmosphere, is taken from the semi-empirical data of Lingenfelter (Ref. 12) for solar minimum, which in turn are based on the measurements of Soberman (Ref. 17) and others and on the neutron diffusion calculation of Lingenfelter (Ref. 12). Figure 5 gives the resulting $\overline{S_n}(x, \lambda)$ for $C^{14}$ production in air, as a function of x, with $\lambda$ serving as the parameter. Figure 6 is a replot of the data in Figure 5 as a function of $\lambda$ with x as the parameter.

## IV. DISCUSSION

Our aim in this report is to attempt to reduce the atmospheric data to a form amenable to comparison with cascade calculations. It is not our aim to derive specific yield functions for use in studying the rigidity dependence of time-variations of the primaries, and the results cannot be so used.

Two characteristics of cascade calculations decrease the accuracy required for the work reported here. Firstly, even for incident energies below 10 or 15 GeV, these calculations tend to give results containing large uncertainties, although the exact magnitude of these uncertainties are usually unknown. This should be especially true when the absorber is made of light elements such as nitrogen and oxygen. Because the model used in calculating the nucleon-nucleus (and pion-nucleus) interactions is a statistical one, the reliability of such interaction calculations on a light nucleus containing so few nucleons is open to serious question. This, in fact, is one reason for the present work; that is, to have atmospheric data for comparison with calculations of nuclear cascades in air (nitrogen and oxygen). Secondly, cascade calculations, especially those made by the Monte Carlo technique are capable of handling very complex geometrical and kinematical situations. Thus, it is a simple matter for the calculations to allow primaries to be incident on the atmosphere, or air absorber, not only vertically but also isotropically, or in accordance with any arbitrary directional distribution that one may prescribe. Although it is still necessary to assume a unique cutoff rigidity at a given geomagnetic latitude while differentiating as in Equation (3), we did not feel it would be necessary to apply the Gross transformation to the atmospheric data $I(x, \lambda)$, as is normally done in deriving specific yield functions. Instead of making the several arbitrary assumptions necessary for the Gross transformation to be applied validly, we ask the cascade calculators to include non-vertical primaries, with their appropriate slightly differing cutoff rigidities and to follow the oblique cascades they induce. This procedure allows one to deal with those atmospheric data for which the Gross transformation is not valid.

Similarly, as already stated in Section II, we do not make any assumptions at present on nucleon-nucleus interactions or on nuclear cascades induced by nuclei heavier than the proton. However, some such assumption

has to be made when the cascade calculations are undertaken, unless of course by that time high-energy nucleon-nucleus interactions should become thoroughly understood. If the same assumption is made as in Method 2 (see Section II), then the cascade calculations must regard a primary nucleus as equivalent to a group of free nucleons, each inducing a nuclear cascade in air independently of the others. The cascade calculators must also remember that because of the different charge-to-mass ratio, these nucleons do not have the same energy as the free cosmic ray protons arriving from the same direction at the same latitude.

In comparing the curves obtained here with cascade calculations, it is necessary to compare any one of the Figures 1 to 6 with the corresponding calculated curves. This is because Figures 1, 3, and 5 do not represent independent empirical data; in other words, the $I(x, \lambda)$ used in deriving Figures 3 and 5 are ultimately based on the same set of empirical data as those used in deriving Figure 1. Therefore, no additional information can be gained on the validity of the cascade calculation by comparing with more than one of these figures (Figures 1 to 6).

Because the Gross transformation was not applied to the input $I(x, \lambda)$ it is difficult to comment on the appearance of the curves in Figures 1 to 6 short of actually comparing them with properly tailored cascade calculations. Despite this, it is obvious that the general trends of the curves in Figures 1 to 6 are similar to the usual trends observed in laboratory experiments in which thick targets are bombarded by monoenergetic protons (References 5 and 6). Thus, as the latitude decreases, i.e., as the rigidity increases, the slope of the $\overline{S_n}$ versus x curves become less steep. This, of course, is only an enhancement of the same trend already present in the input $I(x, \lambda)$ versus x curves.

An interesting feature seen in Figures 1 to 6 is the large increase in $\overline{S_n}$ between 50° and 40° latitude and the lack of significant increase in $\overline{S_n}$ from 30° to 0°. This is easily seen in either the $\overline{S_n}$ versus x curves (Figures 1, 3, and 5) where the curves crowd together at low latitudes, or in the $\overline{S_n}$ versus $\lambda$ curves (Figures 2, 4, and 6), where the curves flatten out at low latitudes. A similar feature was noted by Treiman (Ref. 9). The meaning of such a feature is that as the incident rigidity of the primaries increase to about 10GV, the density of neutrons (and of the stars that produce them) in the cascade doesn't increase very much, and although this roughly holds at least up to an incident rigidity of some 15 GV (near 0° latitude), there is a hint in the curves that $\overline{S_n}$ does increase above 15 GV.

The curves in Figures 1 to 6 do not extend to latitudes greater than $60^{\circ}$, because the primary latitude curve is flat above the latitude "knee". These curves do not extend all the way to $0^{\circ}$ latitude because the slope of the primary latitude curve near $0^{\circ}$ is very small, making the calculation of $S_n$ difficult.

ACKNOWLEDGEMENT

The work reported here was carried out under the direction of Dr. Trutz Foelsche of the National Aeronautics and Space Administration, Langley Research Center, Langley Station, Hampton, Virginia.

We wish to thank Dr. B. S. P. Shen of New York University, consultant to the Space Sciences Laboratory for his advice and assistance in the course of this work.

APPENDIX A

Numerical Operation on the Data

The input data are shown on Figures A1, A2, A3, and A4. We note that the curves on A2, A3, and A4 have the same ordinates but the zeros on the abscissae have been shifted sequentially to the right by 50 grams/$cm^2$.

Curve A1 is the latitude curve of the primary nucleons at the top of the atmosphere. It is necessary to obtain the rate of change of this flux with latitude to follow Method 1. The slope was obtained graphically. These slopes were plotted and a smooth curve drawn through the points. Figure A5 shows the slopes as smoothed. Values of the slopes were then taken from this curve. Since the values of $J_n$ were expressed in nucleons /$cm^2$ sec steradian, we have multiplied by $2\pi$ steradians to obtain the flux incident on the atmosphere, see discussion in Section IV. The slope units then become nucleons/$cm^2$ sec degree latitude.

Figure A2 shows the number of neutrons/$cm^2$ sec as a function of depth in the atmosphere in grams/$cm^2$ where latitude has been used as the parameter producing the several curves. These curves were normalized so that the areas under them would follow the values shown in the table taken from Ref. 12. The factor was calculated

Table A1 - Normalization Data

| Latitude Curve (Degrees) | Area Under the Curve (Neutrons/$cm^2$ sec) |
|---|---|
| 0 | 1.48 |
| 10 | 1.53 |
| 20 | 1.85 |
| 30 | 2.76 |
| 40 | 4.60 |
| 50 | 7.03 |
| 60 | 8.54 |
| 70 | 9.00 |
| 80 | 9.00 |
| 90 | 9.00 |

and found to be 8.84 by using Simpson's rule for finding areas. These curves were measured and redrawn (a sample is shown on Figure A6) as a function of latitude with depth in the atmosphere being the parameter. For these curves the scale was changed frequently for ease in reading. The slope of these curves was measured graphically at ten degree intervals. These values were divided by the readings on curve A5 to give the values, $\overline{S_n}$, as shown in Table AII. These $\overline{S_n}$, values may be plotted in two ways: (1) $\overline{S_n}$ versus depth in the atmosphere, Figure 1, with latitude as the parameter; or (2) $\overline{S_n}$ versus latitude, Figure 2, with depth in the atmosphere as the parameter. Between these two "cross" plots the curves may be smoothed as actually shown.

Figure A3 shows the neutron dose rate as a function of depth in the atmosphere with latitude as the parameter. These data were treated exactly the same as described for Figure A2 above, except for the normalization. The results are shown in Figures 3 and 4.

Figure A4 shows the number of carbon$^{14}$ atoms per gram sec as a function of depth in the atmosphere with latitude as the parameter. These data were treated as described above for Figure A2, except that the normalization factor is 9.00. The results are shown in Figures 5 and 6.

Table AII - Calculated Values for $\overline{S_n}$ in Neutrons/gram/Neucleons/cm$^2$

| Latitude/Depth in Atmosphere | 50* $\times 10^{-2}$ | 200* $\times 10^{-2}$ | 400* $\times 10^{-3}$ | 600* $\times 10^{-3}$ | 800* $\times 10^{-4}$ | 1033* $\times 10^{-4}$ |
|---|---|---|---|---|---|---|
| 5 | 1.24 | 2.49 | 13.38 | 2.51 | 17.38 | 2.51 |
| 10 | 1.84 | 2.03 | 9.20 | 2.25 | 11.71 | 2.04 |
| 20 | 2.39 | 2.12 | 6.58 | 2.33 | 6.99 | 1.83 |
| 30 | 2.94 | 2.21 | 5.85 | 1.98 | 4.73 | 1.22 |
| 40 | 3.45 | 1.75 | 4.78 | 1.11 | 2.57 | .36 |
| 50 | 2.59 | .40 | .96 | .27 | .72 | < .01 |
| 60 | < 0.01 | .07 | .24 | < .01 | < .01 | < .01 |

*grams/cm$^2$

APPENDIX B

Separation of $\alpha$ Particle and Proton Curves

According to Method 2 explained in Section II, we have

$$\frac{dI(x,R)}{dR} = S_1(x,R)\ \frac{dJ_1(R)}{dR} + S_1(x,\tfrac{1}{2}R)\ \sum_Z A_Z\ \frac{dJ_Z(R)}{dR} \qquad \text{(B-1)}$$

In order to find $S_1(x,R)$, one needs to know $J_1$, $J_2$, $J_3$, etc. To simplify matters, we make the further assumption, following Webber and Quenby (Ref. 10), that

$$\sum_Z A_Z K_Z \approx 1, \qquad \text{(B-2)}$$

where $$K_Z \equiv \frac{\frac{dJ_Z(R)}{dR}}{\frac{dJ_1(R)}{dR}} \qquad \text{(B-3)}$$

The above assumption in effect says that half of the primary nucleons arrive at the top of the atmosphere as free protons and the other half arrive locked in nuclei heavier than hydrogen. This is in good agreement with the primary charge spectrum of Webber (Ref. 28), adopted by Webber and Quenby (Ref. 10). The above assumption also implies that the differential rigidity spectra of the various charge components of the primaries all have the same shape; this is not strictly true, but is good enough in view of the approximate and illustrative nature of this Appendix. With assumption (B-2), Equation (B-1) reduces to

$$\frac{dI(x,R)}{dR} = \left[S_1(x,R) + S_1(x,\tfrac{1}{2}R)\right]\ \frac{dJ_1(R)}{dR} \qquad \text{(B-4)}$$

Compare with Equation (3) of Section II to obtain

$$\frac{\overline{S_n}(x,R)}{S_1(x,R) + S_1(x,\frac{R}{2})} = \frac{\frac{dJ_1(R)}{dR}}{\frac{dJ_n(R)}{dR}} = \frac{1}{\rho} \tag{B-5}$$

since the shapes of all primary differential rigidity spectra are alike, the ratio $\rho$ is a constant for all R. The ratio was obtained at the top of the atmosphere Lingenfelter (Ref. 12) and found to be 0.44/0.23 or 1.91.

Following Webber and Quenby (Ref. 10) we may write

$$S_1(x,R) = \rho \overline{S_n}(x,R) - S_1(x,\frac{R}{2}) \tag{B-6}$$

and with the proviso that

$$S_1(x,\frac{R}{2}) = \rho \overline{S_n}(x,\frac{R}{2}) - S_1(x,\frac{R}{4}) \tag{B-7}$$

etc. we find that

$$S_1(x,R) = \rho \left[ \overline{S_n}(x,R) - \overline{S_n}(x,\frac{R}{2}) - \overline{S_n}(x,\frac{R}{4}) - \overline{S_n}(x,\frac{R}{8}) - \ldots \right] \tag{B-8}$$

This is an infinite sum which may be cutoff when the remainder becomes neglectable according to some criteria.

For our case, the $\overline{S_n}(x,R)$ have been calculated at certain discrete values of the latitude (hence cutoff rigidity) so that another procedure is given here to make use of the discrete points. A series of equations may be written such as

$$S_1(x,R_1) = \rho\,\overline{S_n}(x,R_1) - S_1(x,\frac{R_1}{2})$$

$$S_1(x,R_2) = \rho\,\overline{S_n}(x,R_2) - S_1(x,\frac{R_2}{2}) \qquad \text{(B-9)}$$

$$S_1(x,R_3) = \rho\,\overline{S_n}(x,R_3) - S_1(x,\frac{R_3}{2})$$

etc.

Looking at Figure 2 and Table AII we find that six values of $\overline{S_n}(x,R)$ were calculated (at $\lambda$ = 5, 10, 20, 30, 40, and 50) which can be used to obtain a similar number of $S_1(x,R)$. However, there must be a relation between the cutoff rigidity and the latitude in order to use Equation B-9.

Quenby and Webber (Ref. 27) shows this relation. Because of the approximations we have made in treating the data and in smoothing the graphs, we have used the dipole approximation rather than the series approximation for the Earth's magnetic field. This is equivalent to taking the relation

$$R(\lambda) = R(o)\cos^4\lambda \qquad \text{(B-10)}$$

Table BI gives the cutoff rigidities according to reference 27 and the latitudes corresponding to the half rigidity of points.

Table BI - Rigidity-Latitude Relation

| Latitude | Cutoff Rigidity in BV | $\frac{1}{2}$ Rigidity in BV | Corresponding Latitude |
|---|---|---|---|
| 0° | 15.0 | 7.5 | 32° 46' |
| 5 | 14.8 | 7.4 | 33° 06' |
| 10 | 14.2 | 7.1 | 34° 06' |
| 20 | 11.0 | 5.5 | 37° 48' |
| 30 | 8.5 | 4.25 | 43° 15' |
| 40 | 5.2 | 2.6 | 49° 54' |
| 50 | 2.5 | 1.25 | 57° 17' |

Fortunately, all latitudes fall within our computed points so that interpolations may be made. According to Table AII we note that $\overline{S_n}\,(x, 60^o)$ is generally much smaller than $\overline{S_n}\,(x, 50^o)$. Since $S_1\,(x, R)$ will follow the shape of the $\overline{S_n}$ curve, we may take $S_1\,(x, 60^o)$ as zero (or a small value depending upon the $\overline{S_n}\,(x, 60^o)$ during interpolation. Linear interpolation will be used in this work. According, we may write expressions such as

$$S_1\,(x, 33^o\,06') = \left[S_1\,(x, 40) - S_1\,(x, 30)\right] \frac{3.10}{10} - S_1\,(x, 30) \qquad \text{(B-11)}$$

The equations for $S_1\,(x, R)$ in B-9 may now be written using constants a, b, c, d, e, and f for the interpolation ratios such as 3.10/10 in Equation B-11.

$$\begin{aligned}
S_1\,(x, 5) &= \rho\,\overline{S_n}\,(x, 5) - S_1\,(x, 30)(1-a) - S_1\,(x, 40)\,a \\
S_1\,(x, 10) &= \rho\,\overline{S_n}\,(x, 10) - S_1\,(x, 30)(1-b) - S_1\,(x, 40)\,b \\
S_1\,(x, 20) &= \rho\,\overline{S_n}\,(x, 20) - S_1\,(x, 30)(1-c) - S_1\,(x, 40)\,c \\
S_1\,(x, 30) &= \rho\,\overline{S_n}\,(x, 30) - S_1\,(x, 40)(1-d) - S_1\,(x, 50)\,d \qquad \text{(B-12)} \\
S_1\,(x, 40) &= \rho\,\overline{S_n}\,(x, 40) - S_1\,(x, 50)\,e \qquad \text{(2 - e)} \\
S_1\,(x, 50) &= \rho\,\overline{S_n}\,(x, 50) - S_1\,(x, 60)\,f \qquad \text{(2 - f)}
\end{aligned}$$

There are six equations but seven unknowns. For the reason stated above we will assume that $S_1\,(x, 60)$ is small enough to be neglected. This is roughly the same approximation as was made in the series of Equation B-8.

Equations B-12 were solved to obtain $S_1\,(x, R)$ for the data in Table AII; that is, for $\overline{S_n}$ of Figures 1 and 2. Values are plotted in Figures B1 and B2. By the use of Equation B-1 values of $S_2\,(x, R)$ may be calculated; Figures B3 and B4 are plots of those data.

REFERENCES


1. A. Reetz, Jr., Editor, Proceedings of the Second Symposium on Protection Against Radiations in Space NASA SP-71 (1965).

2. R. G. Alsmiller, Jr., ORNL-TM-1298 (1965) invited paper at First Symposium on Accelerator Radiation Dosimetry and Experience, Nov. 1965.

3. C. D. Zerby and W. E. Kinney, ORNL-TM-1038 (1965), Nuclear Instr. and Meth. (in press).

4. D. B. Ebeogln and K. M. Wainis, paper to be presented at American Geophysical Union Meeting, April 1966, Washington, D. C.

5. H. Bindewald et. al. Nucl. Instr. and Meth. Vol. 32, 45 (1965).

6. B. S. P. Shen, NASA SP-71 (1965), edited by A. Reetz, Jr., p. 357.

7. R. G. Alsmiller, Jr. and J. Barish, ORNL-3852 (1965).

8. H. V. Neher, Progr. in Cosmic-Ray Physics, Vol. I (North-Holland Publishing and Interscience, (1952), p. 243 (esp. pp. 307-310).

9. S. B. Trieman, Phys. Rev., Vol. 86, p. 917 (1952).

10. W. R. Webber and J. J. Quenby, Phil. Mag; Ser. 8, Vol. 4, p. 654 (1959).

11. R. D. Albert, C. Gilbert, and W. N. Hess, J. Geophys. Res., Vol. 67, p. 3537 (1962).

12. R. E. Lingenfelter, Revs. of Geophys., Vol. 1, p. 35 (1963).

13. H. V. Neher and H. R. Anderson, J. Geophys. Res., Vol. 67, p. 1309 (1962).

14. J. A. Lockwood, J. Geophys. Res., Vol. 65, p. 19 (1960).

15. W. C. Lin, D. Venkatesan, and J. A. Van Allen, J. Geophys. Res., Vol. 68, p. 4885 (1963).

16. S. N. Milford, AIAA Journal, Vol. 3, p. 193 (1964).

17. R. K. Soberman, Phys. Rev., Vol. 102, p. 1399 (1956).

18. D. C. Rose, K. B. Fenton, J. Katzman, and J. A. Simpson, Canadian J. Phys., Vol. 34, p. 968 (1956).

19. J. A. Simpson and W. C. Fagot, Phys. Rev., Vol. 90, p. 1068 (1953).

20. J. A. Simpson, Phys. Rev., Vol. 83, p. 1175 (1951).

21. P. Meyer and J. A. Simpson, Phys. Rev., Vol. 99, p. 1517 (1955).

22. J. J. Lord, Phys. Rev., Vol. 81, p. 901 (1951).

23. B. S. P. Shen, General Electric Technical Information Series R64SD1 (1964).

23a. W. W. Brown, Phys. Rev., Vol. 93, p. 528 (1954).

23b. F. W. Bullock, Proc. Phys. Soc., Vol. A70, p. 134 (1957).

24. D. Lal, P. K. Malhotra, and B. Peters, J. Atm. Terr. Phys., Vol. 12, p. 306 (1958).

25. R. C. Haymes, W. P. Reidy, and S. A. Korff, J. Phys. Soc. Japan, Vol. 17, Suppl. A-II, p. 115 (1962).

26. H. W. Patterson, W. N. Hess, B. J. Moyer, and R. W. Wallace, Health Phys., Vol. 2, p. 69 (1959).

27. J. J. Quenby and W. R. Webber, Phil. Mag., Ser. 8, Vol. 4, p. 90 (1959).

28. W. R. Webber, Nuovo Cimento, Vol. 4, p. 1285 (1956).

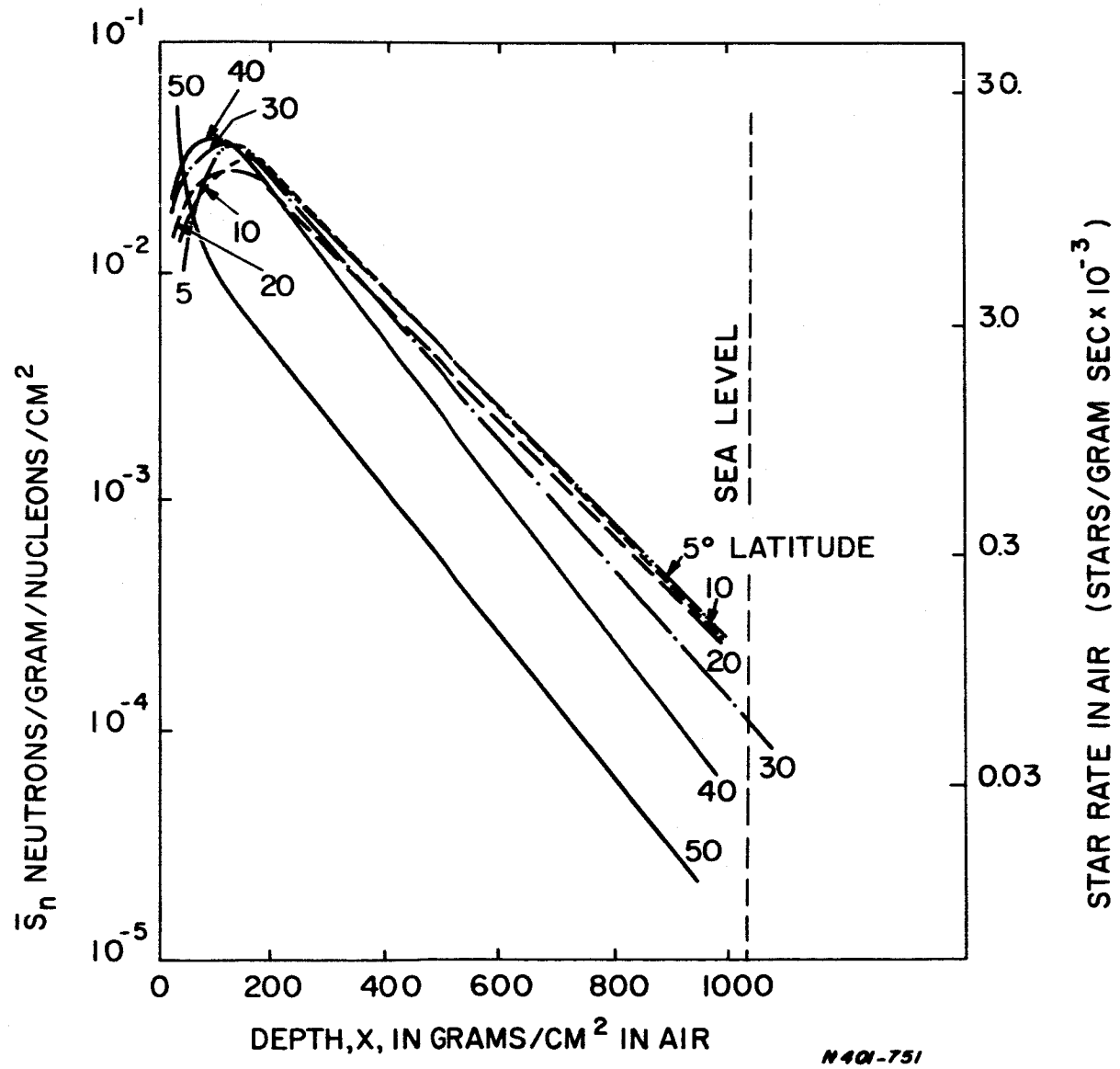


Fig. 1. Calculated Values of $\bar{S}_n$ (x, R) vs Depth for Neutrons and Stars in Air

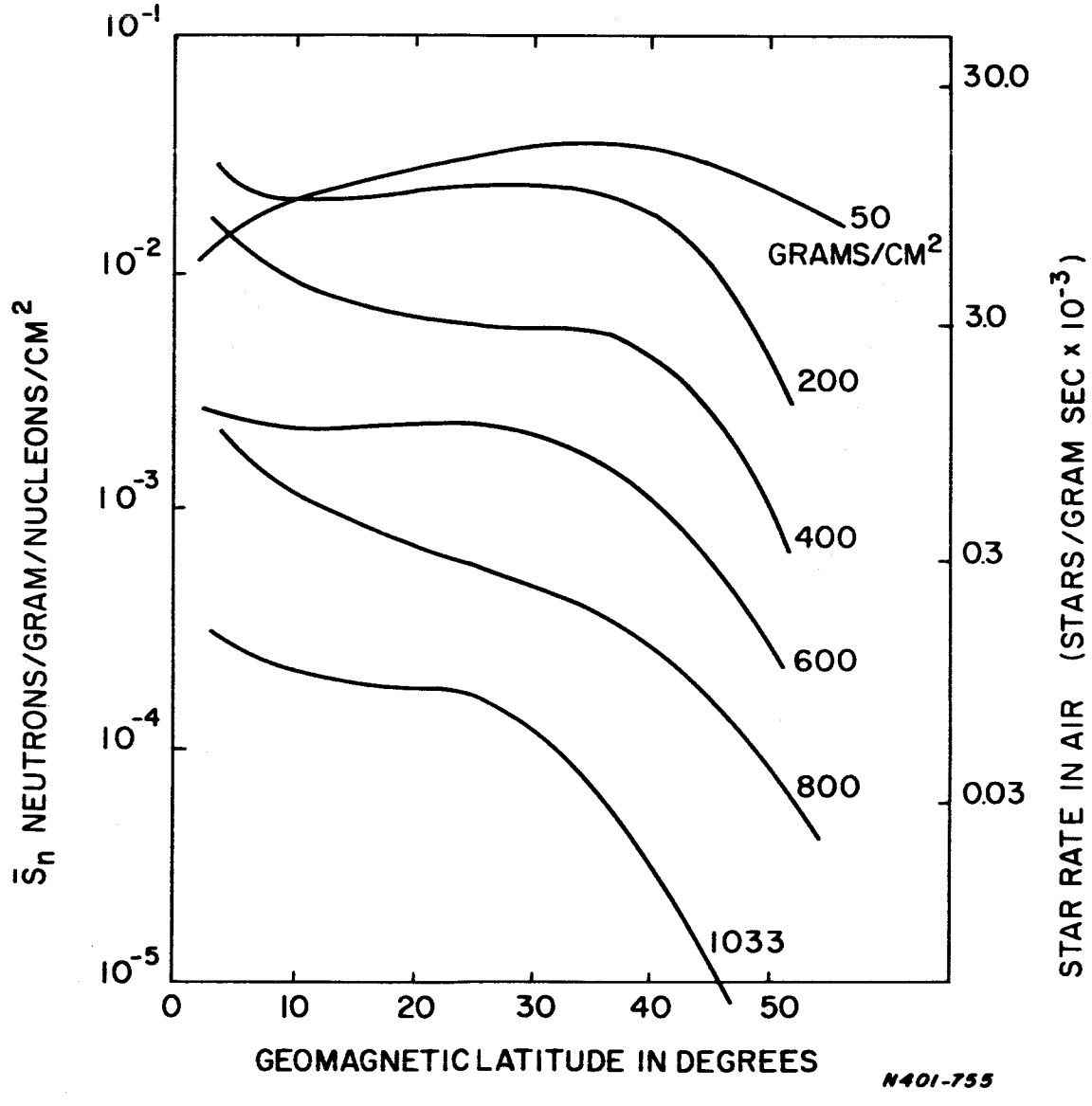


Fig. 2. Calculated Values of $\bar{S}_n$ (x, R) vs Latitude for Neutrons and Stars in Air

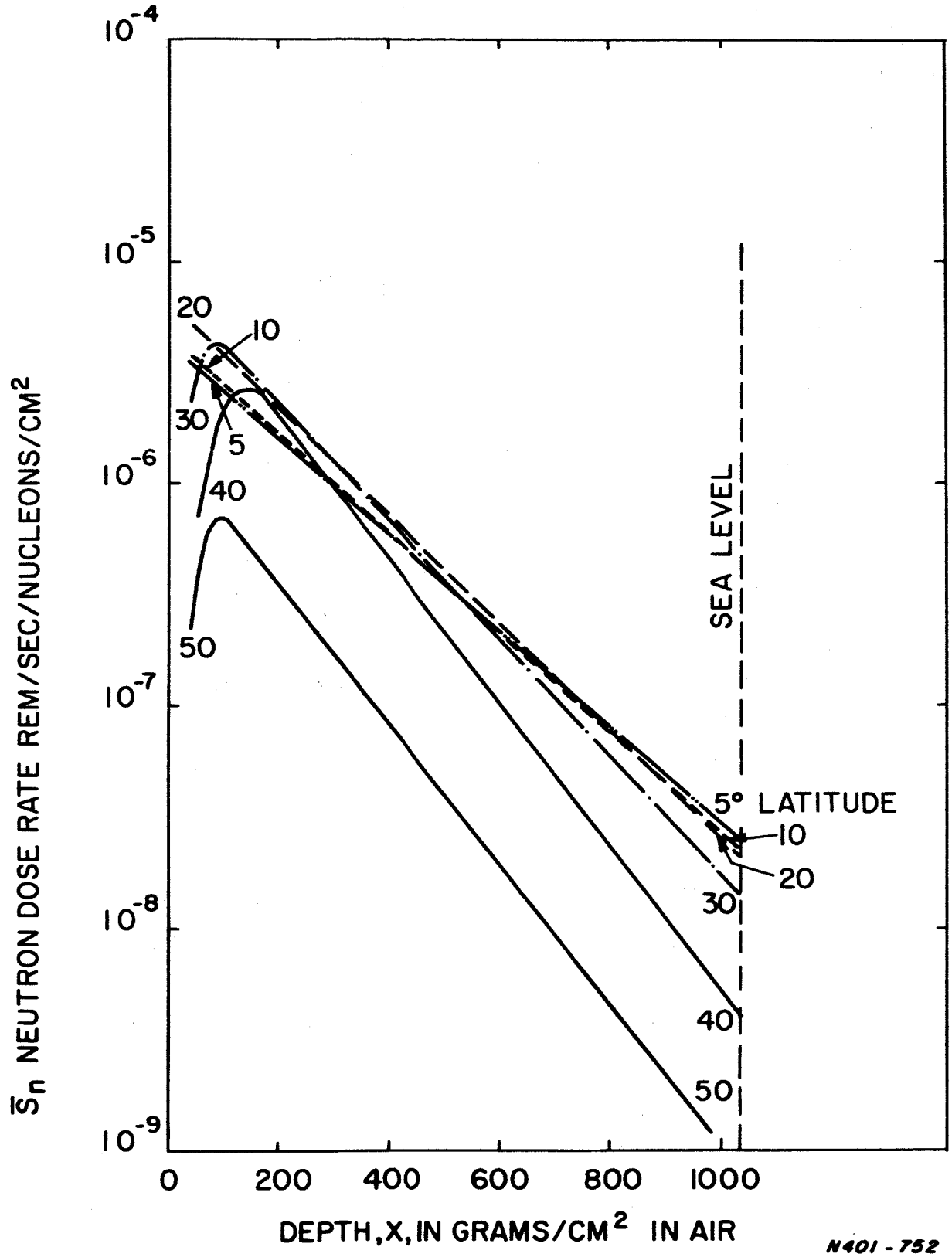


Fig. 3. Calculated Values of $\bar{S}_n$ (x, R) vs Depth for Neutron Dose Rate In Air

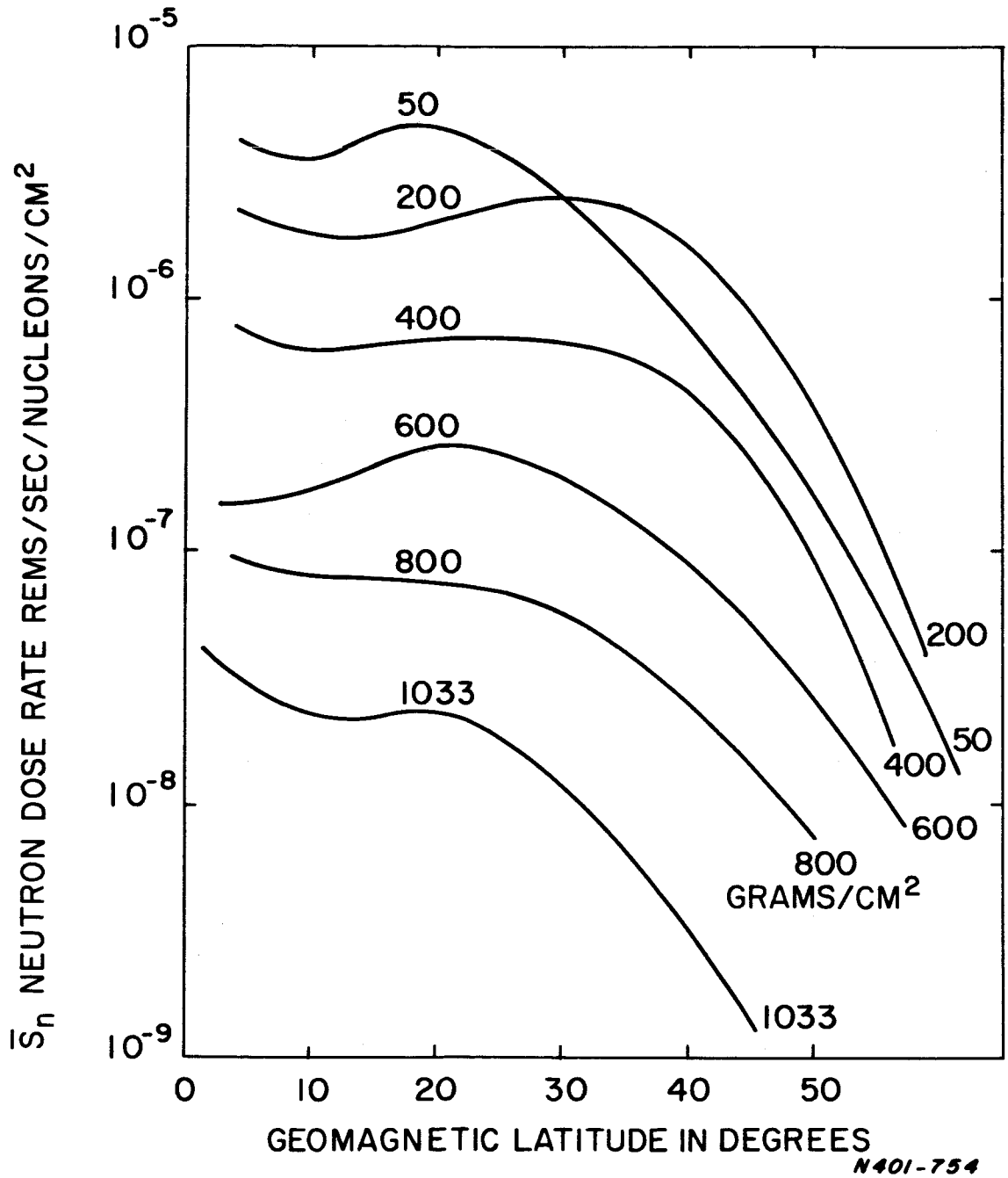


Fig. 4. Calculated Values of $\bar{S}_n$ (x, R) vs Latitude for Neutron Dose Rate in Air

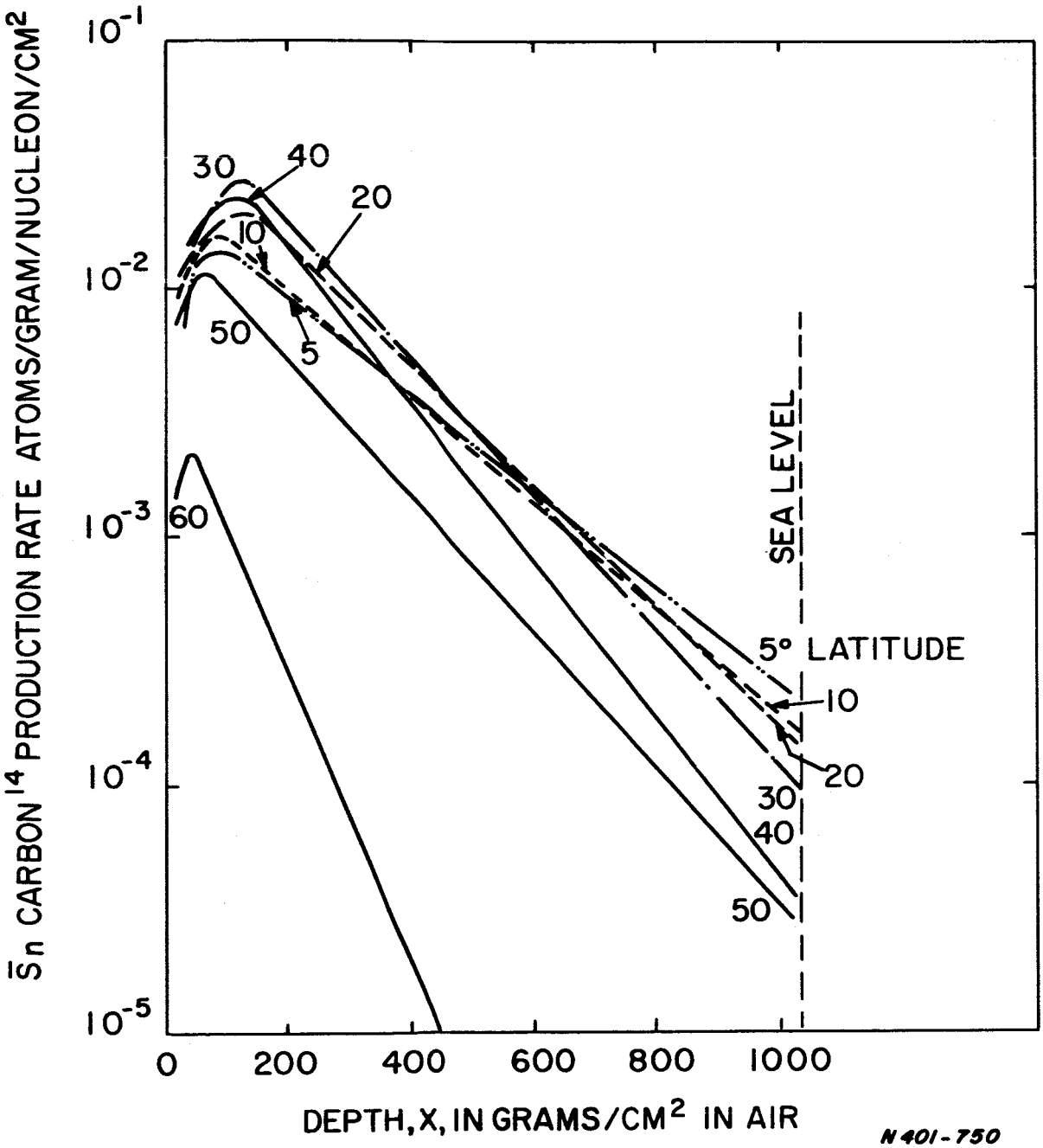


Fig. 5. Calculated Values of $\bar{S}_n$ (x, R) vs Depth for Carbon $^{14}$ Atom Production Rate in the Air

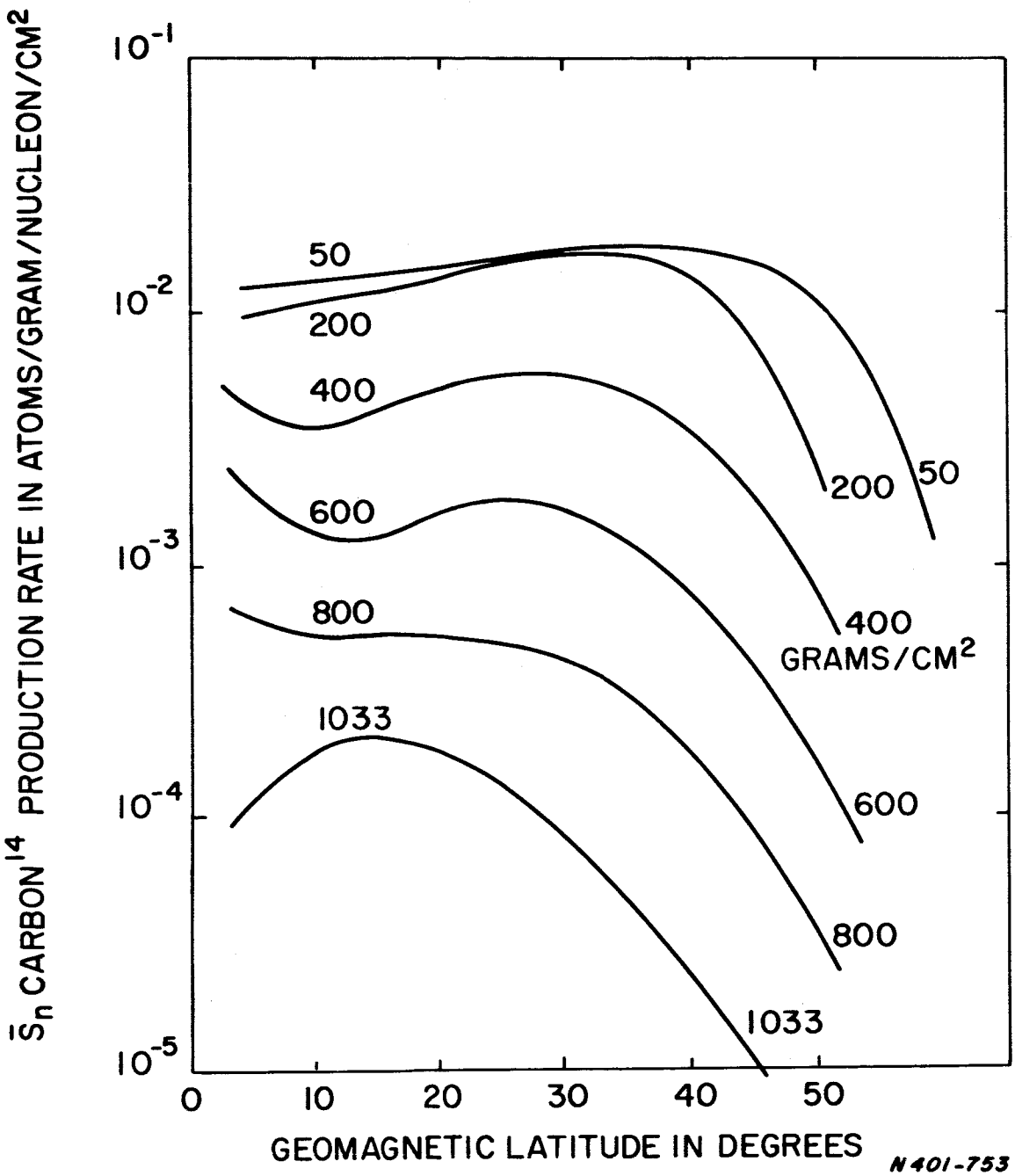


Fig. 6. Calculated Values of $\bar{S}_n$ (x, R) vs Latitude for Carbon $^{14}$ Atom Production Rate in Air

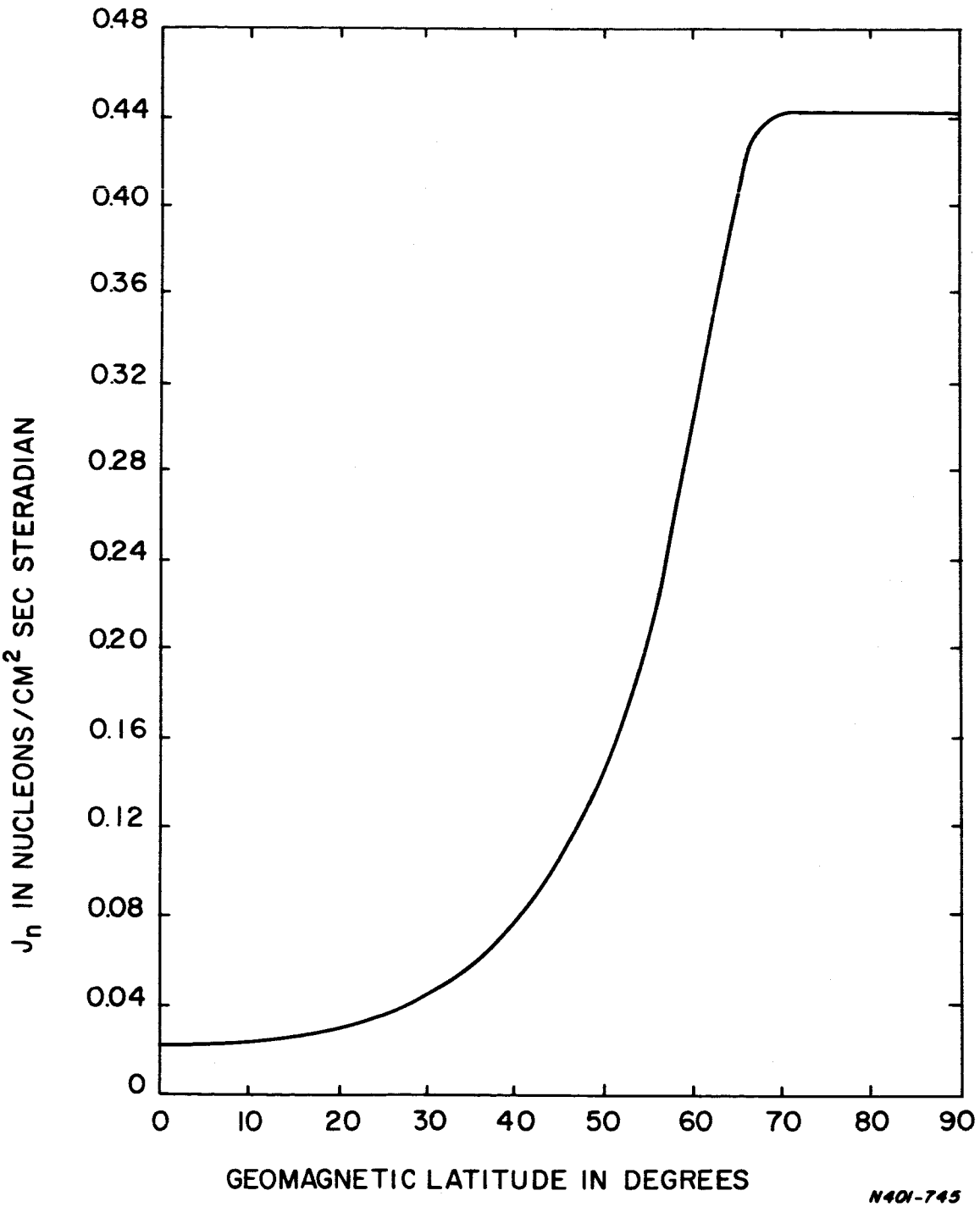


Fig. A1. Nucleon Flux incident upon Top of the Atmosphere

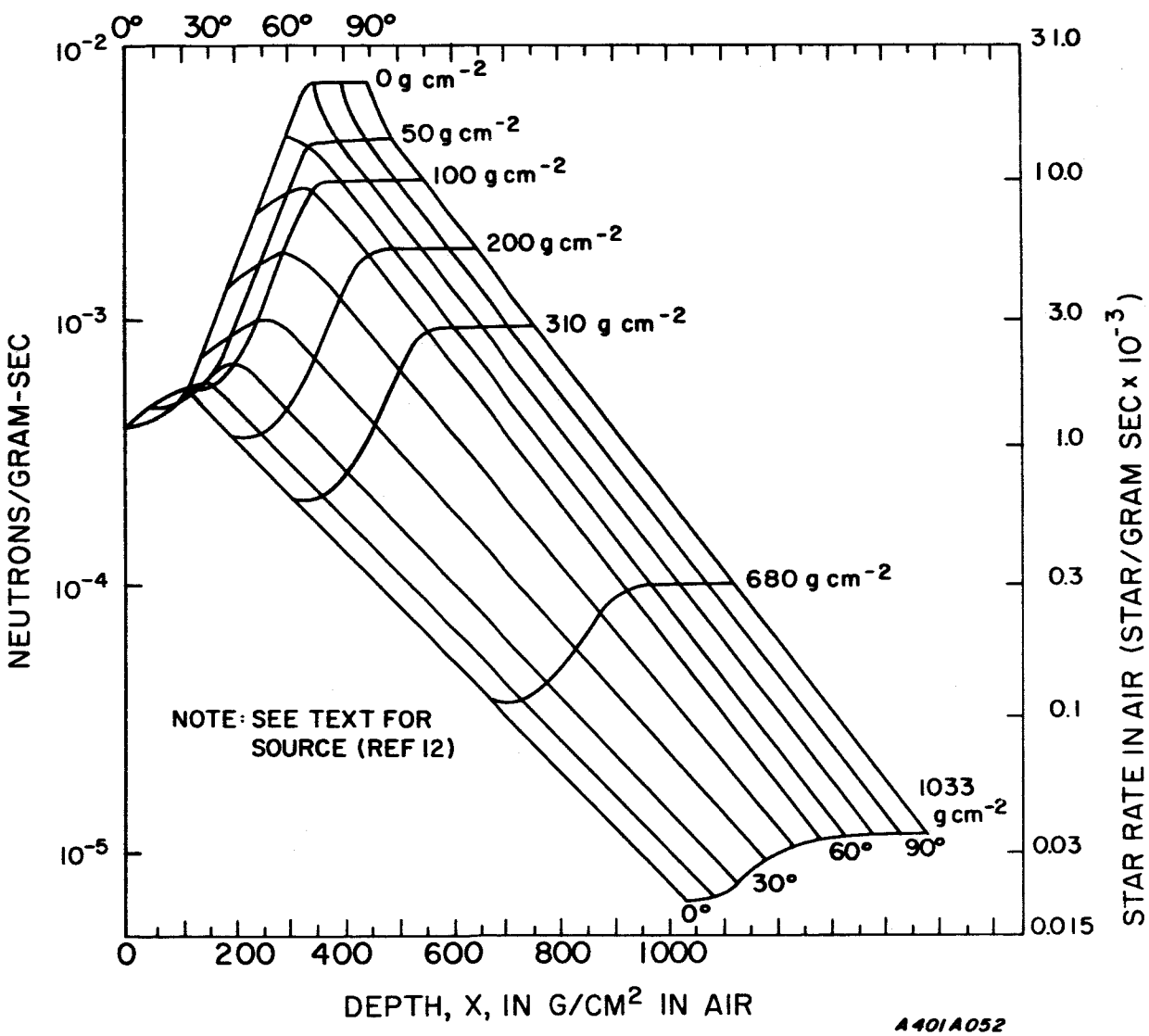


Fig. A2. Solar Minimum Cosmic Ray Neutron Production Rate

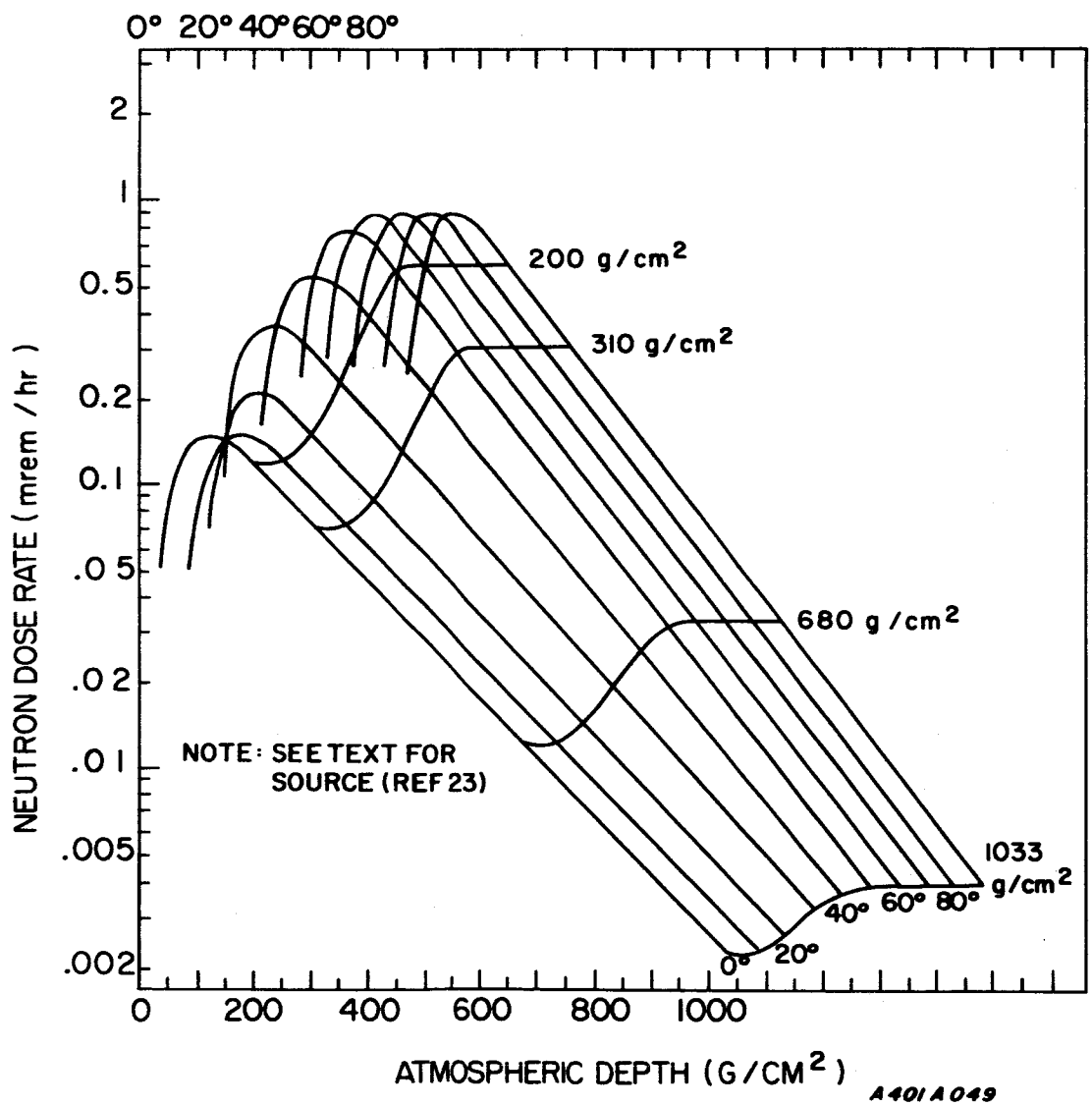


Fig. A3. Neutron Dose Rate in the Atmosphere

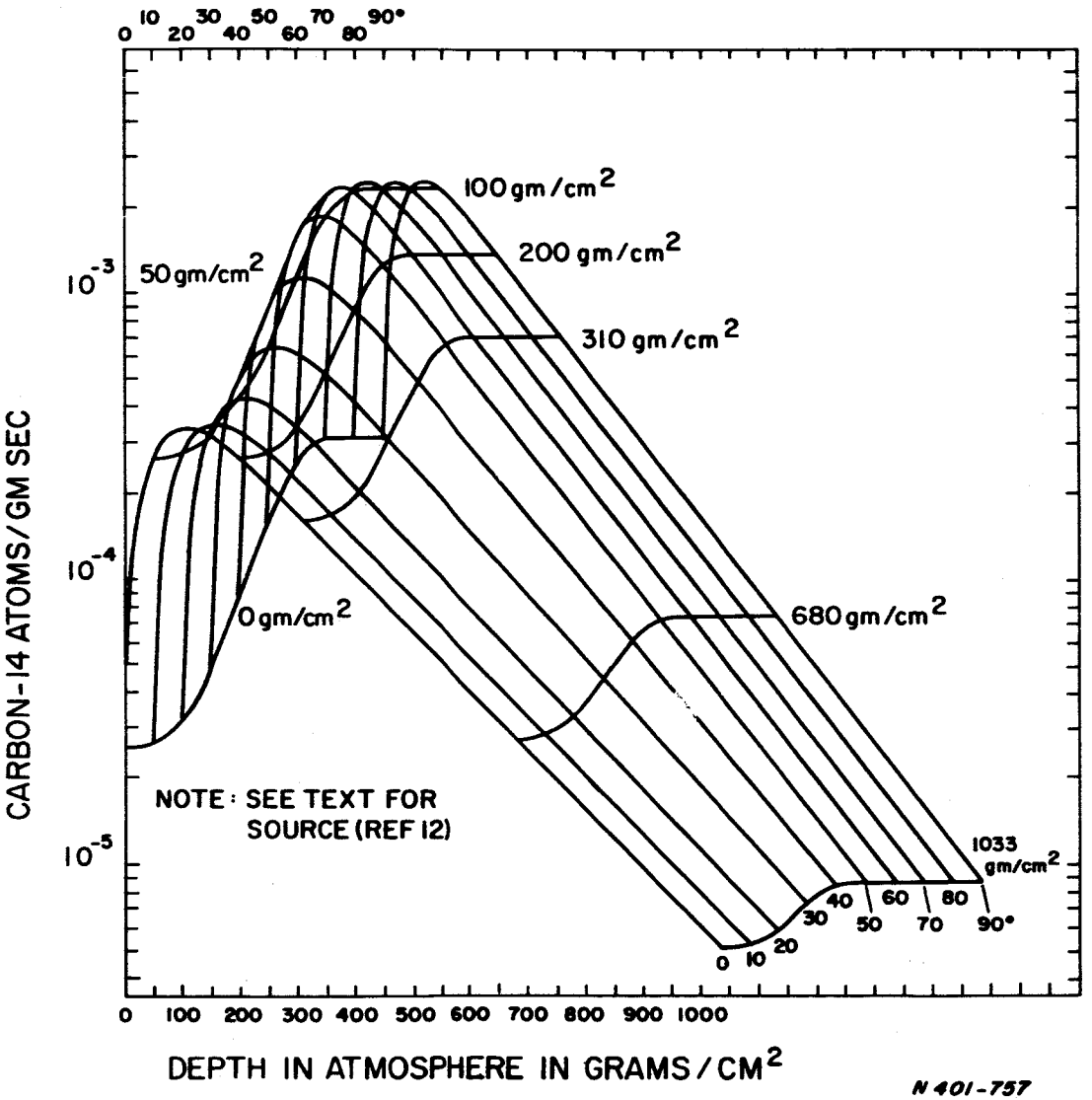


Fig. A4. Carbon $^{14}$ Production Rate in the Atmosphere at Solar Minimum

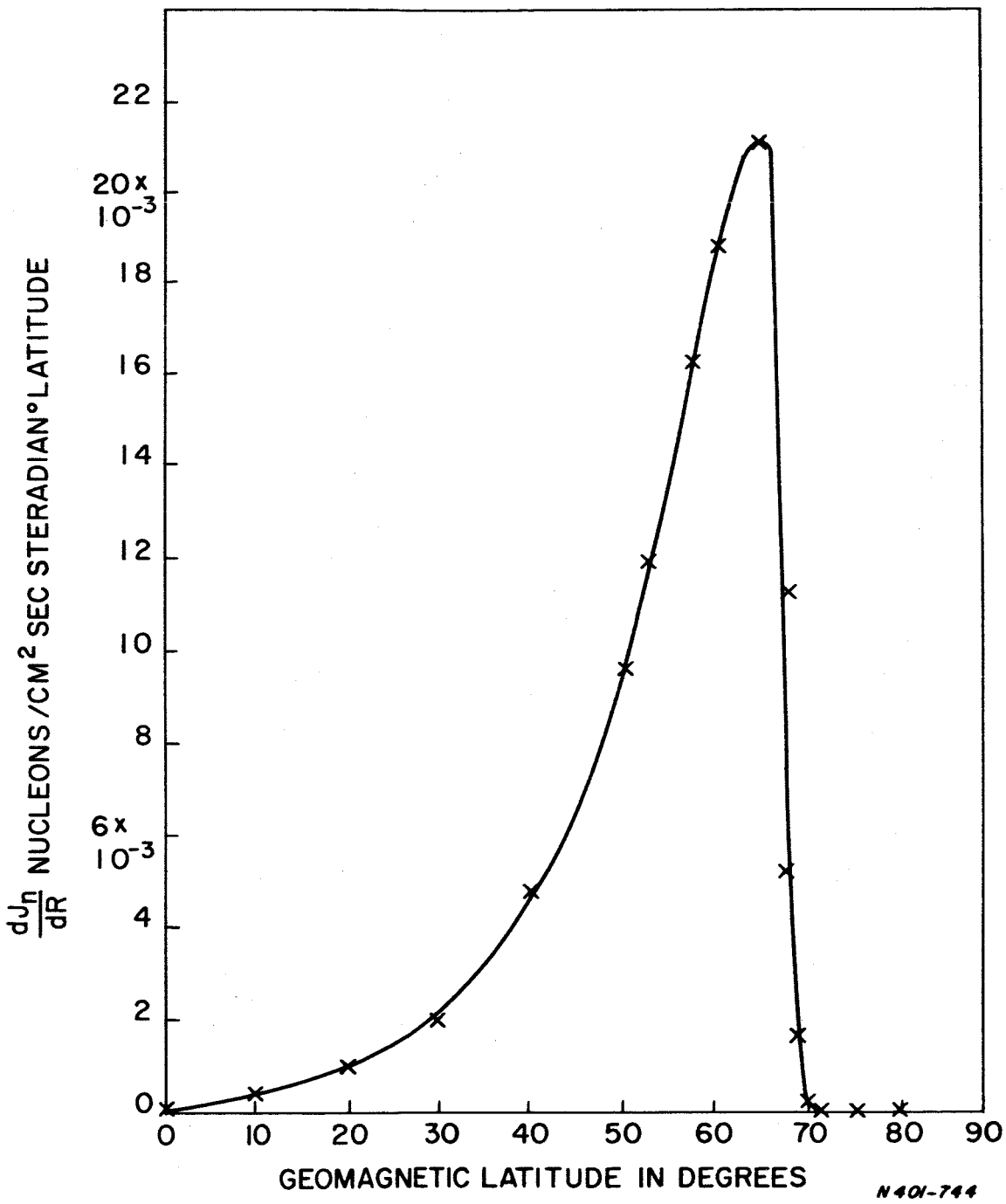


Fig. A5. Rate of Change of Primary Flux with the Latitude

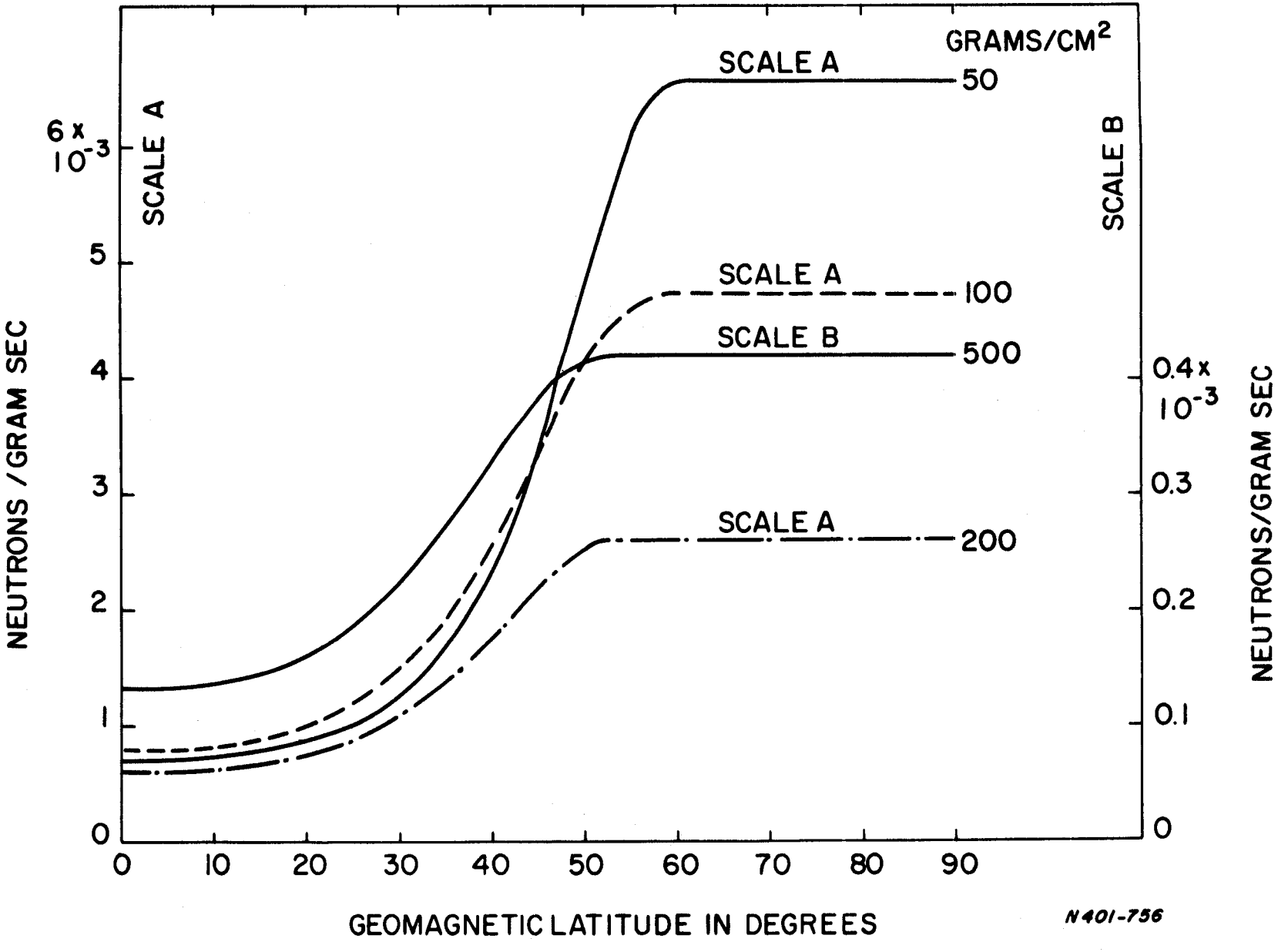


Fig. A6. Neutron Density Measured in Air vs Latitude During Solar Minimum

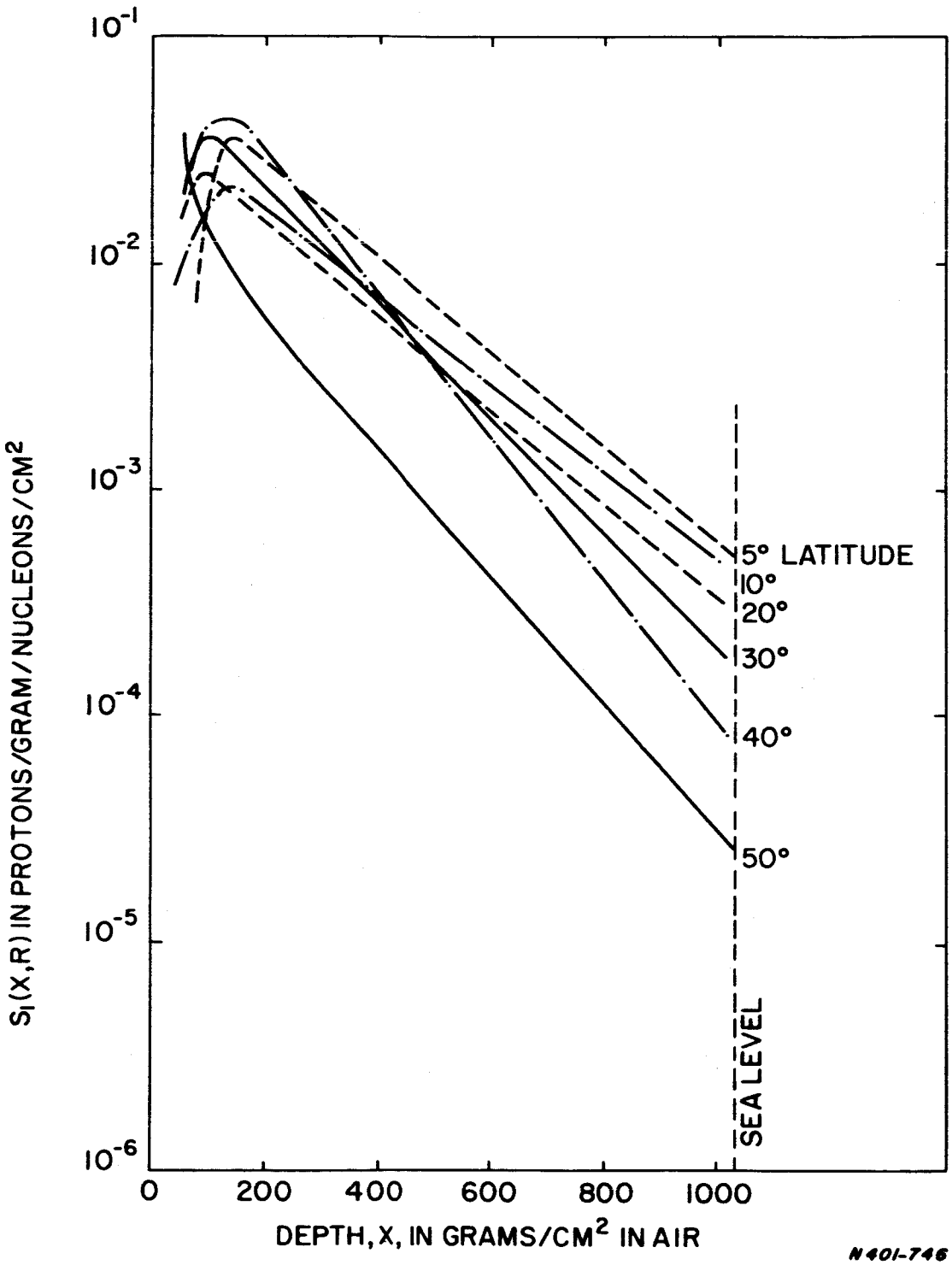


Fig. B1. Calculated Values of $S_1$ (x, R) vs Depth in Air

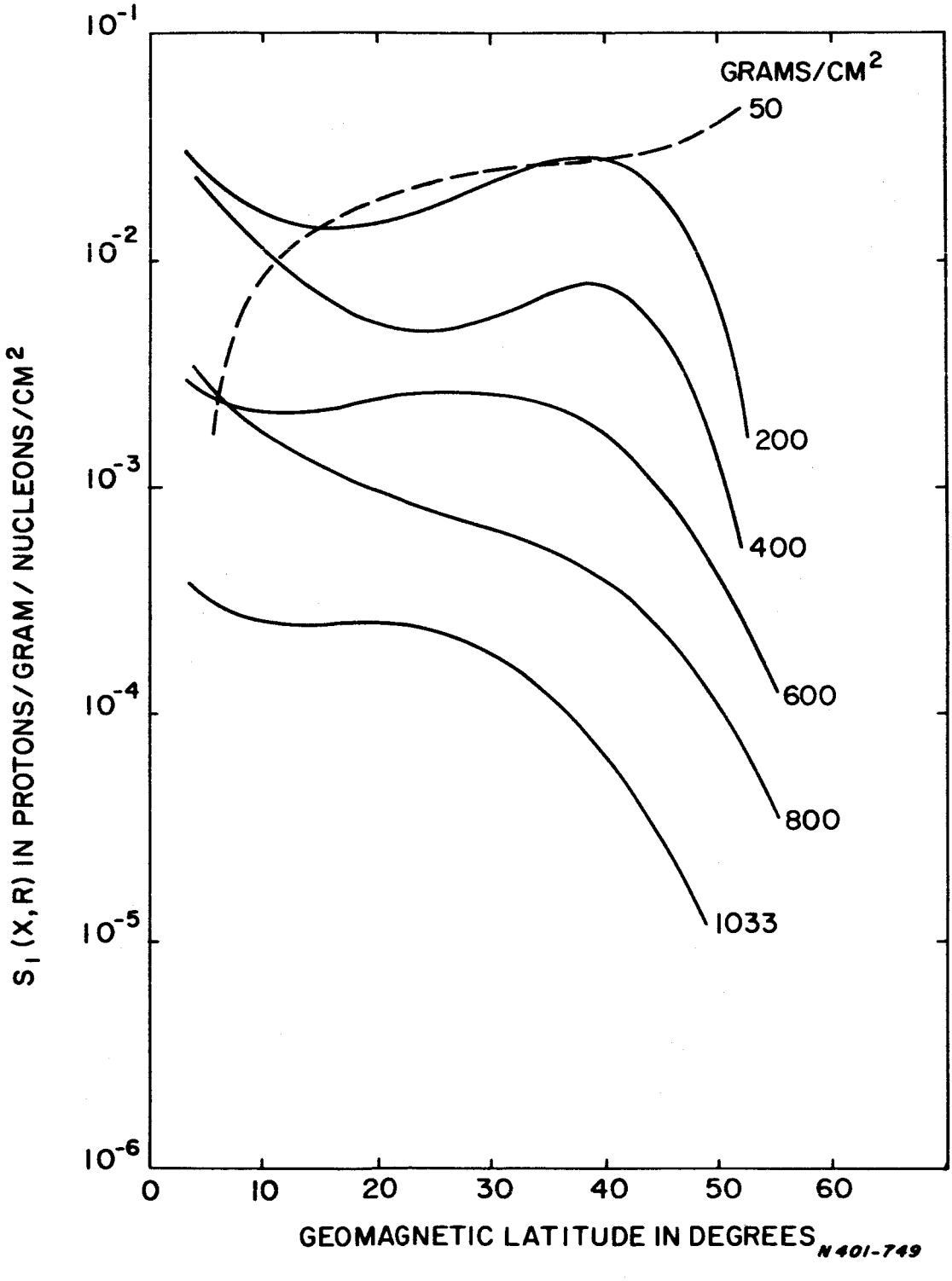


Fig. B2. Calculated Values of $S_1$ (x, R) vs Latitude in Air

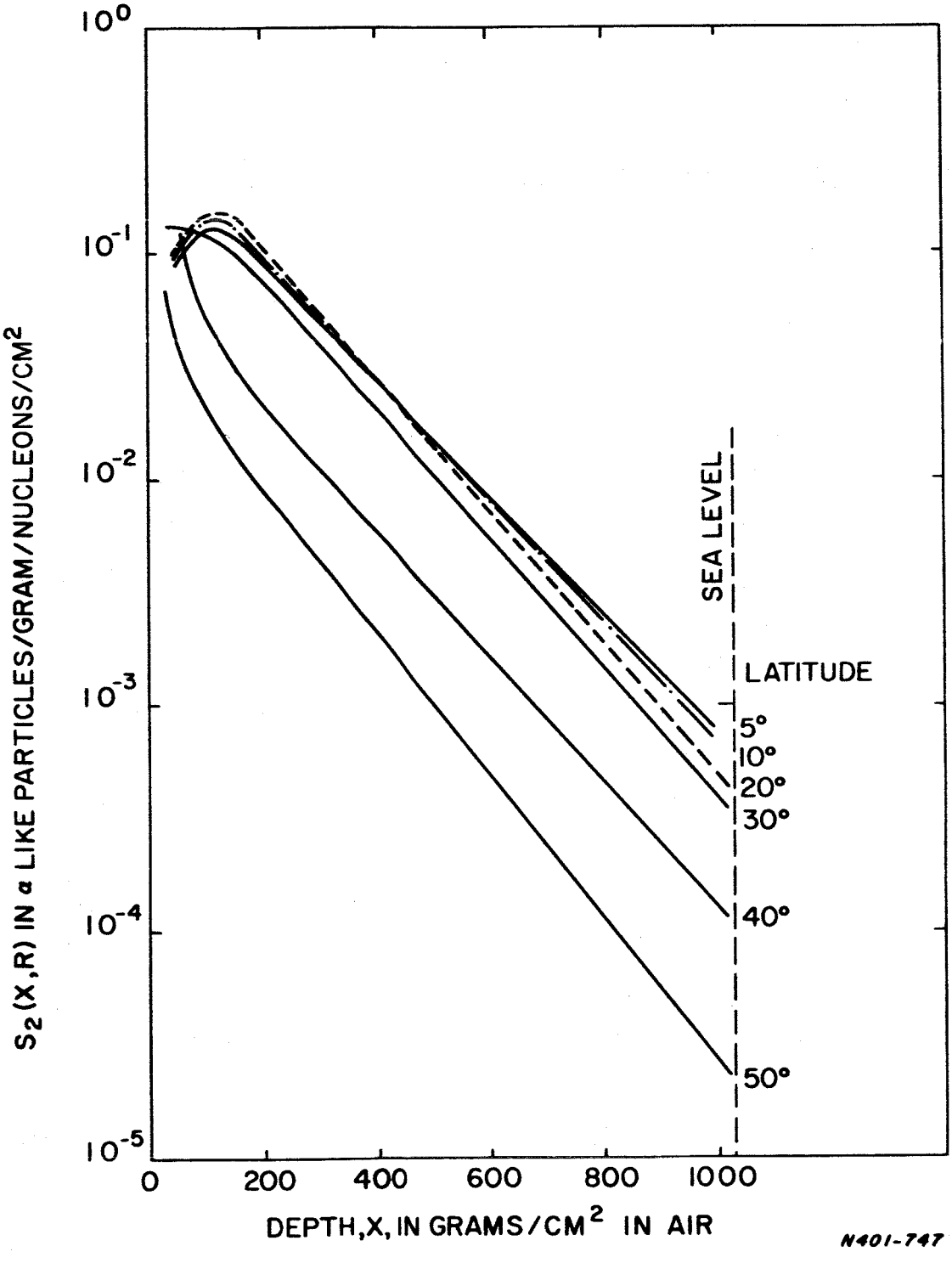


Fig. B3. Calculated Values of $S_2$ (x, R) vs Depth in Air

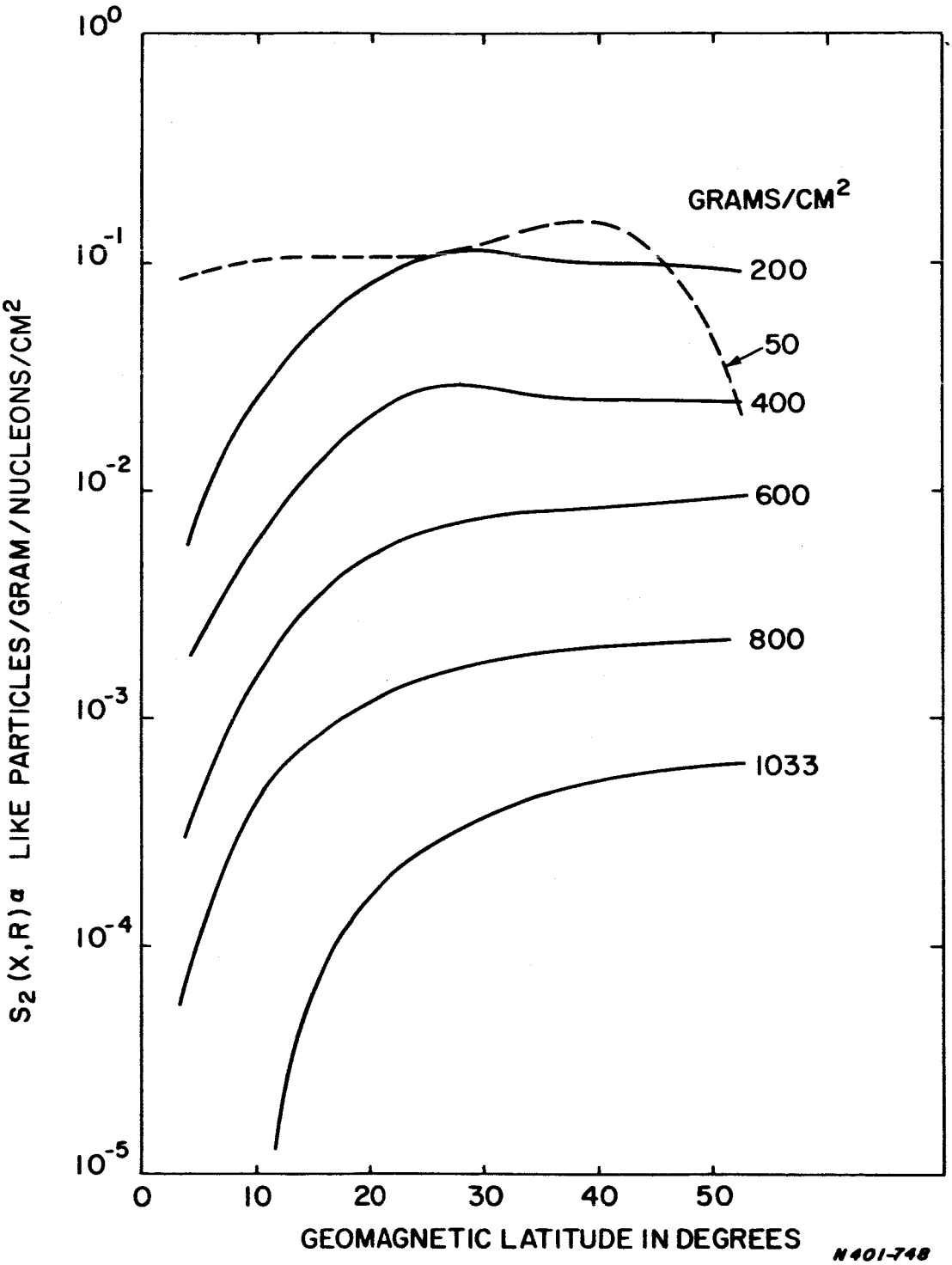


Fig. B4. Calculated Values of $S_2$ (x, R) vs Latitude in Air